Atmos. Chem. Phys., 25, 425–439, 2025
https://doi.org/10.5194/acp-25-425-2025

Atmospheric Chemistry and Physics
Open Access
EGU

Enhanced sulfate formation in mixed biomass burning and sea-salt interactions mediated by photosensitization: effects of chloride, nitrogen-containing compounds, and atmospheric aging

Rongzhi Tang[1,2], Jialiang Ma[3], Ruifeng Zhang[4], Weizhen Cui[1], Yuanyuan Qin[5], Yangxi Chu[6], Yiming Qin[1], Alexander L. Vogel[3], and Chak K. Chan[4]

[1]School of Energy and Environment, City University of Hong Kong, Hong Kong SAR, China
[2]Shenzhen Research Institute, City University of Hong Kong, Shenzhen 518057, China
[3]Institute for Atmospheric and Environmental Sciences, Goethe University Frankfurt, 60438 Frankfurt am Main, Germany
[4]Division of Physical Science and Engineering, King Abdullah University of Science and Technology (KAUST), Thuwal 23955-6900, Kingdom of Saudi Arabia
[5]College of Resources and Environment, University of Chinese Academy of Sciences, Beijing 100049, China
[6]State Key Laboratory of Environmental Criteria and Risk Assessment, Chinese Research Academy of Environmental Sciences, Beijing 100012, China

Correspondence: Chak K. Chan (chak.chan@kaust.edu.sa)

Received: 21 August 2024 – Discussion started: 29 August 2024
Revised: 31 October 2024 – Accepted: 2 November 2024 – Published: 13 January 2025

Abstract. Discrepancies persist between modeled simulations and measured sulfate concentrations in the marine boundary layer, especially when the marine air is influenced by biomass burning plumes. However, there has been a notable dearth of research conducted on the interactions between sea-salt aerosol and biomass burning plumes, impeding a comprehensive understanding of sulfate formation. This work studied sulfate formation by mixing real biomass burning (BB) extracts and NaCl, mimicking internal mixtures of BB and sea-salt particles. BB–NaCl particles had a significantly higher sulfate formation rate than incense burning (IS)–NaCl particles. For fresh particles, the sulfate formation rate followed the trend of corn straw (CS)–NaCl > rice straw (RS)–NaCl > wheat straw (WS)–NaCl > IS–NaCl. The filter sample aging was achieved by exposure to OH• generated from UV irradiation. After aging, RS–NaCl particles exhibited the highest enhancement in sulfate formation rates among all the BB–NaCl particles due to interactions between RS and NaCl. Bulk aqueous experiments spiked with NaCl using mixtures of model photosensitizers (PSs) and nitrogen-containing organic compounds (NOCs), pyrazine (CHN), and 4-nitrocatechol (CHON) revealed positive effects of chloride in the PS–CHON system and negative effects in the PS–CHN system in sulfate formation. Our work suggests that BB reaching or near coastal areas can affect sulfate formation via photosensitizer-mediated reactions, potentially exacerbating air pollution.

Published by Copernicus Publications on behalf of the European Geosciences Union.

1 Introduction

Recent fire outbreaks in areas like Canada, Amazonia, and southeast Australia, together with the increased fire frequency and intensity reports in areas like the western USA have highlighted the risks of fire, especially biomass burning (BB), to human health and climate change (Bond et al., 2013; Andreae, 2019; Jones et al., 2022). As an agricultural powerhouse, China boasts immense agricultural crop yields, especially in rice, wheat, and corn, throughout the country. These crop residues are frequently burned in rural areas for cooking and heating purposes, as well as for land preparation after harvest, resulting in the substantial production of light-absorbing species, such as brown carbon (BrC) (Chen et al., 2017). Recent studies have reported that specific BrC species from biomass burning, including vanillin (VL), acetovanillone, syringaldehyde (SyrAld), and naphthalene-derived secondary organic aerosol (Teich et al., 2016; Li et al., 2024; Liu et al., 2020; X. Wang et al., 2021), can act as photosensitizers (PSs) and oxidize SO_2 to sulfate (Zhou et al., 2023; Liang et al., 2024). Atmospheric processes like aging or long-range transport can alter the chemical compositions and optical properties of PSs and hence affect the sulfate formation potential (You et al., 2020; Li et al., 2019). Sea-salt aerosol (SSA), with its high particulate matter loadings and extensive surface area, plays a significant role in interfacial and multiphase reactions with reactive gases, thereby impacting the global radiation balance and air quality in marine and coastal areas (Gantt and Meskhidze, 2013; Chi et al., 2015). Prior research has identified several secondary sulfate formation pathways in SSA, e.g., multiphase SO_2 oxidation by O_3 (Alexander et al., 2012), the coexistence of NO_2 (Zhang and Chan, 2023), PSs (Tang et al., 2023), chlorine–PS synergistic effects (Zhang and Chan, 2024), and Cl and OH radicals generated by chlorine photoactivation (Cao et al., 2024). The chlorine and chloride studies are particularly interesting as they highlight the importance of NaCl-based photochemistry in sulfate formation.

SSA can frequently mix with organic matter through processes such as sea-to-air emission, photochemical oxidation, and atmospheric transport (H. Liu et al., 2023). Previous studies have observed elevated sulfate concentrations in coastal regions when air masses have passed through inland areas due to intensive BB or other anthropogenic emissions, suggesting the possible interactions between the SSA (primarily sodium chloride) and anthropogenic emissions (Qiu et al., 2019; Huang et al., 2018; Wu et al., 2022). Van Pinxteren et al. (2015) observed an increase in sulfate concentration ($2.26\,\mu g\,m^{-3}$) during the RV *Maria S. Merian* cruise as it approached the African mainland, in contrast to the marine-origin aerosol ($1.59\,\mu g\,m^{-3}$), showing significant influence of BB. Hence, mixing of sea-salt and biomass burning aerosols can lead to secondary aerosol production in coastal regions.

Transmission electron microscopy (TEM) studies indicate that most coastal particles are internally mixed, showing a higher proportion of organic and salt mixtures in the presence of biomass burning aerosols, accompanied by an increase in sulfate (Dang et al., 2022; Li et al., 2003). However, discrepancies persist between modeled simulations and measured sulfate concentrations in the marine boundary layer (MBL; Yu et al., 2023). The interactions of sea-salt and BB aerosols, especially in multiphase reactions, can potentially unravel the intricate chemistry of sulfate formation in the BB-affected MBL. Hence, internal mixtures of inorganic salt and water-soluble organic carbons are often used in reaction studies (Tan et al., 2024).

The two main atmospheric water systems in the MBL are wet aerosol (droplets in our case) and cloud/fog (bulk aqueous solutions); both droplet and aqueous reactions are relevant to studying multiphase sulfate formation within the MBL (Ruiz-Lopez et al., 2020; Herrmann, 2003). Typically, droplet reactions are characterized by high ionic strength (up to 10 M), low liquid water content (10^{-7}–$10^{-3}\,cm^3\,m^{-3}$), and a high surface-to-volume ratio, whereas aqueous reactions exhibit the opposite characteristics. Additionally, droplet experiments can encompass certain interfacial reaction pathways that may occur in the atmosphere, especially in submicron particles (Ruiz-Lopez et al., 2020).

Previous studies have detected a significant proportion of nitrogen-containing organic compounds (NOCs), including nitroaromatics (CHON) and reduced-nitrogen species (CHN) in biomass burning plumes, wildfires, and ambient samples (Zhong et al., 2024; Y. Wang et al., 2017; Song et al., 2022; Cai et al., 2020). These NOCs are considered ubiquitous contributors to BrC and can affect global climate and human health. Moreover, recent research has discovered aerosol pollution in marine background regions, with high levels of NOCs when air masses are transported from wildfires or biomass burning events nearby (Zhong et al., 2024; Qin et al., 2024). These NOCs, combined with reactive gases, may mix with SSA and impact regional air quality in coastal zones. Therefore, it is essential to further investigate the interactions between NOCs, reactive gases, and SSA.

In this study, we performed in situ droplet and bulk aqueous solution reaction experiments using BB extract–NaCl mixtures to explore the possible interplay between biomass burning and marine aerosols in coastal areas. BB was derived from the burning of rice straw (RS), wheat straw (WS), and corn straw (CS) as well as incense burning (IS). The aims of this study are to (i) compare the differences in sulfate formation among different kinds of BB–NaCl particles and BB extracts, (ii) examine the impacts of OH• aging on sulfate formation across different BB–NaCl particles and BB extracts, and (iii) investigate the role of NOCs and chloride ions in BB-extract-mediated sulfate formation.

2 Materials and methods

2.1 Burning experiments

Three types of commonly used biomass (RS, WS, and CS) were cut into small uniform pieces (~ 10 cm in length) and dried. About 100 g of the dried biomass materials (~ 10 % moisture content) was then introduced into a traditional iron stove commonly used in rural areas (Fig. S1 in the Supplement). The stove was covered with a hood, and the biomass was ignited using a propane lighter. The BB smoke generated was collected onto 90 mm quartz filters at 0.9 m^3 min^{-1} for 10 min by a custom-made aerosol sampler under mixed combustion conditions (include flaming and smoldering, modified combustion efficiency (MCE) $0.85 \leq \Delta[CO_2]/(\Delta[CO_2]+\Delta[CO]) \leq 0.95$) (Ting et al., 2018). The sampler was placed 1 m above the ground and connected to a $PM_{2.5}$ sampling head through a sampling pump. For incense burning (IS), laboratory-generated smoldering smoke was collected on 47 mm quartz filters at a flow rate of ~ 6.0 L min^{-1} for 80 min using a stainless-steel combustion chamber. Note that the different combustion modes of IS and BB are intentionally used to represent real-world combustion conditions. Our previous study demonstrated that IS was representative of BB based on GC × GC (two-dimensional gas chromatography) chromatograms and pixel-based partial least-squares discriminant analysis (Tang et al., 2023). Hereafter, we will use BB to represent both the real BB materials and the surrogate materials (IS) unless otherwise specified. After sampling, the collected BB samples (fresh BB) were wrapped by pre-baked aluminum foil (550 °C for 6 h) and stored at −20 °C until further analysis.

To achieve atmospheric OH• aging, the collected fresh BB filter samples were placed in a pre-flushed chamber (zero air, more than 24 h) and illuminated with UV lamps for 40 min. We used lamps of 185 and 254 nm, the combination of which has been widely used in oxidation flow reactor design and experiments for mimicking atmospheric OH• aging conditions (Peng and Jimenez, 2020; Rowe et al., 2020; Tkacik et al., 2014; Hu et al., 2022). The estimated OH exposure was $\sim 2.0 \times 10^{12}$ molecules cm^{-3} s, equivalent to an atmospheric aging period of 15 d (assuming an average atmospheric OH concentration of 1.5×10^6 molecules cm^{-3}) (Mao et al., 2009). Detailed characterization of the OH exposure can be found in our previous study (Tang et al., 2023). We will discuss the sulfate formation of these fresh and OH• aged samples later.

2.2 Materials and instrumentation

Aqueous stock solutions of BB samples were prepared by dissolving the collected filters in ultrapure water and subjecting them to ultrasonication in a cooled-water bath three times, each for 20 min. The resulting water extracts of the BB were then filtered through 0.22 µm PTFE filters and stored in brown vials at 4 °C in a refrigerator. The anions, i.e., the chloride, sulfate, and nitrate of the BB extracts, were analyzed by Dionex ion chromatography (ICS-1100, USA). An aliquot (~ 0.5 mL) of the BB or IS extracts was used for water-soluble organics detection by ultra-high-performance liquid chromatography (UHPLC; Thermo Fisher Scientific, Dionex UltiMate 3000) coupled with high-resolution Orbitrap Fusion Lumos Tribrid mass spectrometry (Orbitrap HRMS, Thermo Fisher Scientific, USA). The particulate organic matter was characterized by directly heating the filter samples using a thermal desorption module (TDS 3, GERSTEL) coupled to a comprehensive two-dimensional gas chromatograph–mass spectrometer (GCMS-TQ™8050 NX, Shimadzu, Japan). UV–Vis spectrometry (UV-3600, Shimadzu, Japan) was employed to examine the absorbance of BB extracts. Total organic carbon (TOC) was measured by a total carbon analyzer (TOC-L CPH, Shimadzu, Japan). Metal concentrations were measured by inductively coupled plasma–mass spectrometry (ICP-MS, Agilent 7800). Detailed analysis can be found in Sect. S1 in the Supplement. Aqueous stock solution of sodium chloride (≥ 99.8 %, Unichem) was prepared by dissolving the corresponding salt in ultrapure water to obtain a concentration of 1 M. The study utilized high-purity-grade synthetic air and nitrogen supplied by Linde HKO Ltd., while sulfur dioxide was obtained from Scientific Gas Engineering Co., Ltd.

2.3 Multiphase and aqueous-phase reactions of S(IV)

In SO_2 uptake experiments, the stock solution of BB (fresh and aged) extracts was premixed with sodium chloride solution (1 M) at a volume ratio of 1 : 1, and the solutions had a pH of 4–6. A droplet generator (model 201, Uni-Photon Systems, Inc.) was then utilized to deposit droplets onto a hydrophobic substrate (model 5793, YSI Inc.) for SO_2 uptake experiments. Reactive SO_2 uptake experiments were performed via a flow cell–in situ Raman system at controlled room temperature (23–25 °C). The top and bottom quartz windows of the flow cell were used for Raman analysis and UV irradiation, respectively. The light experiment was performed using a xenon lamp (model 6258, ozone-free, 300 W, Newport), with a photon flux of 9.8×10^{15} photons cm^{-2} s^{-1} at 280–420 nm received by particles in the flow cell (Zhang and Chan, 2023). Identical experiments were conducted in the dark with the lights off and the experimental area kept in complete darkness. The relative humidity (RH) inside the flow cell was adjusted to 80 % by mixing dry and wet synthetic air or nitrogen. The particles were then equilibrated at 80 % RH for over 60 min and remained liquid throughout the experiment period. SO_2 was introduced into the system to reach a concentration of 8.0 ppm. The prescribed size used in our in situ Raman research was 60 ± 5 µm. Despite using particles for droplet experiments that were larger than ambient fine particles, we employed the SO_2 uptake coefficient (γ_{SO_2}) as a kinetic parameter to account for the particle size

effects. Comprehensive calculation of γ_{SO_2} can be found in our previous studies (Gen et al., 2019b, a; Tang et al., 2023; R. Zhang et al., 2020).

Aqueous-phase photochemical reactions were performed using a quartz photo reactor (Go et al., 2023, 2022). Specifically, a 500 mL solution containing 100 ppm bisulfite and 1 ppm BB TOC extracts was continuously mixed using a magnetic stirrer throughout the experiments. Note that the 1 ppm BB TOC and 100 ppm bisulfite align well with the atmosphere-relevant ranges in aqueous aerosols, fog, and clouds, where PS concentration can reach hundreds of micromolar and total sulfur concentration can exceed several millimolar (Anastasio et al., 1997; Guo et al., 2012; Shen et al., 2012; Rao and Collett, 1995). To achieve air-saturated conditions, synthetic air was continuously introduced into the solutions at a flow rate 0.5 L min^{-1} throughout the experiments. The above-described mixed solutions were then exposed to radiation via the same xenon lamp (light intensity of 1318 mW cm^{-2}) as in the droplet experiments. Samples were collected at 1 h intervals for a total of 8 h for sulfate and bisulfite analysis using ion chromatography. Unlike droplet experiments, NaCl was not added to the bulk solution in most studies, unless specified otherwise.

3 Results and discussion

3.1 Enhanced sulfate production in BB–NaCl droplets compared to IS–NaCl droplets

As no sulfate was detected under dark conditions for any of the experiments, we have focused on the light experiments. Figure 1 depicts the sulfate production by (panel a) fresh BB–NaCl droplets and (panel b) aged BB–NaCl droplets as a function of time in the presence of light, air, and SO_2 at 80 % RH. Our previous study (Tang et al., 2023) found significantly higher sulfate formation of IS–NaCl droplets compared to NaCl droplets. Here, we only focus on the comparison of sulfate formation between different kinds of BB–NaCl droplets and IS–NaCl droplets. Regardless of whether the extracts were fresh or aged, the sulfate production by BB–NaCl droplets was higher than IS–NaCl droplets. Specifically, sulfate formed by fresh (F) BB–NaCl droplets followed the trends of CS_F–NaCl (16.8 ± 2.6 mM $(ppmC)^{-1}$) > RS_F–NaCl (9.8 ± 0.1 mM $(ppmC)^{-1}$) > WS_F–NaCl (4.2 ± 0.2 mM $(ppmC)^{-1}$) > IS_F–NaCl (0.8 mM $(ppmC)^{-1}$) after illumination for 1080 min. In aged (A) samples, while BB_A–NaCl is more efficient than IS_A–NaCl in sulfate formation, the order of sulfate formation was different from that of the fresh samples: RS_A–NaCl (35.2 ± 0.6 mM $(ppmC)^{-1}$) > CS_A–NaCl (13.0 ± 0.1 mM $(ppmC)^{-1}$) > WS_A–NaCl (6.0 ± 1.6 mM $(ppmC)^{-1}$) > IS_A–NaCl (0.6 mM $(ppmC)^{-1}$). The sulfate enhancement factors of RS_F–NaCl, WS_F–NaCl, and CS_F–NaCl compared to IS_F–NaCl after 18 h of SO_2 uptake ($Sulfate_{BB_F-NaCl/IS_F-NaCl}$) were 11.7, 5.0, and 20.0, respectively. The enhancement of sulfate can also be observed in aged BB samples, with values of 54.3, 9.2, and 20.1 for RS_A–NaCl, WS_A–NaCl, and CS_A–NaCl, respectively. The lower sulfate formation of IS–NaCl droplets compared to BB–NaCl droplets can be explained by the significantly higher TOC concentration of IS due to the incomplete and smoldering combustion (Table S1 in the Supplement). The TOC concentration of the IS extracts (> 550 mg L^{-1}) was nearly an order of magnitude higher than that of the BB extracts (34.0–69.9 mg L^{-1}), and the sum of anions per water-soluble organic carbon (WSOC) exhibited a more than 10-fold increase in BB extracts compared to IS extracts. Previous studies have confirmed that the smoldering condition of BB results in significantly more organic compounds and fewer ions than the flaming condition (Y. Wang et al., 2020; Fushimi et al., 2017; Kalogridis et al., 2018; Kim et al., 2018). Additionally, a significantly higher polycyclic aromatic hydrocarbon (PAH) proportion (12.2 %–16.6 % by intensity) in BB compared to IS (∼ 5.0 %) were observed by GC × GC–mass spectrometry (MS). G. Huang et al. (2022) reported higher PAHs in BB particles (CS, WS, and RS > 262.5 mg kg^{-1} and > 3.7 % of organic matter) than in IS particles (3.3 mg kg^{-1}, 0.9 % of organic matter) (Song et al., 2023). Fushimi et al. (2017) and Kim et al. (2021) demonstrated that more PAHs can be emitted under flaming than smoldering conditions. PAHs like pyrene, fluoranthene, and phenanthrene have been recognized as PSs (Jiang et al., 2021; Yang et al., 2021) and are mainly from combustion processes, e.g., pyrosynthesis from aliphatic and aromatic precursors in biomass burning processes, and the constituents vary with temperatures and oxygen contents (Pozzoli et al., 2004). The higher percentage of PAHs in BB together with the collection procedure (mixed combustion and higher temperature for real BB and smoldering and lower temperature for IS) suggested that the BB materials would generate more PAHs at high temperatures and may contribute to sulfate formation.

Table 1 and Fig. S2 present the reactive (γ_{SO_2}) and normalized reactive SO_2 uptake coefficients ($n\gamma_{SO_2}$) of different BB–NaCl droplets. The γ_{SO_2} values obtained in our study are 0.9×10^{-6}–6.6×10^{-6}, which are consistent but fall on the low side of the reported heterogeneous SO_2 oxidation processes, including nitrate photolysis (10^{-6}–10^{-5}) (Gen et al., 2019b), transition metal ion (TMI)-catalyzed oxidation (10^{-6}–10^{-4}) (Zhang et al., 2024), NO_2/O_3 oxidation (10^{-6}–10^{-4}) (S. Zhang et al., 2021; Zhang and Chan, 2023), and peroxide oxidation (10^{-6}–10^{-1}) (S. Wang et al., 2021; Ye et al., 2018; Yao et al., 2019). Additionally, the reported γ_{SO_2} in our study aligns well with the results obtained from ambient samples in Beijing (Y. Zhang et al., 2020). The large discrepancy of the reported γ_{SO_2} values can be attributed to the differences in aerosol components, particle size, RH, SO_2, and oxidant concentrations. Higher $n\gamma_{SO_2}$ values were found for fresh and aged real BB–NaCl droplets than IS–NaCl droplets, following the trends of CS_F–NaCl (8.8×10^{-8} $(ppmC)^{-1}$) > RS_F–NaCl (6.2×10^{-8} $(ppmC)^{-1}$) > WS_F–NaCl (2.0×10^{-8} $(ppmC)^{-1}$) > IS_F–NaCl ($0.61 \times$

10^{-8} (ppmC)$^{-1}$) and RS_A–NaCl (2.2×10^{-7} (ppmC)$^{-1}$) > CS_A–NaCl (6.2×10^{-8} (ppmC)$^{-1}$) > WS_A–NaCl (3.5×10^{-8} (ppmC)$^{-1}$) > IS_A–NaCl (0.46×10^{-8} (ppmC)$^{-1}$), respectively.

In our previous study, we observed a significant increase in sulfate formation in IS–NaCl droplets compared to NaCl droplets, which we attributed to PSs present in the IS (Tang et al., 2023). Considering the fact that BB–NaCl droplets produced sulfate more efficiently than IS–NaCl droplets and NaCl droplets, we explore the underlying mechanisms driving this phenomenon. Possible reasons include nitrate (from BB extracts or newly formed) photolysis; [Cl^-–H_3O^+–O_2] photoexcitation (Cl^- from BB extracts); H_2O_2 oxidation; black carbon (BC)-catalyzed oxidation; reactive-nitrogen-species oxidation; and organics-driven pathways, e.g., HCHO, photosensitizing components, organic peroxide, and TMI-organic complexes (Ye et al., 2023).

Since there was no nitrate peak in our Raman spectra in all experiments, the potential impact from nitrate photolysis was excluded. Besides, the very low Cl^- concentration (0.0002–0.001 M) in the original BB extracts (compared to 1 M NaCl, Table S1) has minimized the influence of chloride photoexcitation of [Cl^-–H_3O^+–O_2] (Cl^- from BB extracts) on the sulfate formation. Reactive nitrogen species, e.g., NO_x, HONO, and NH_3, were neither introduced nor detected in our system, indicating that the oxidation pathway involving reactive nitrogen species was insignificant. Additionally, the water extraction process excluded the possibility of BC-catalyzed oxidation. The absence of sulfate formation in dark conditions ruled out the involvement of direct H_2O_2 oxidation and organic peroxide oxidation pathways. The concentrations of TMI did not exhibit a consistent relationship with the sulfate formation observed in both BB_F–NaCl and BB_A–NaCl droplets (Fig. S3), suggesting that the TMI-catalyzed oxidation pathway may not be responsible for the observed phenomenon. Therefore, the most probable reason for the enhancement of sulfate formation by BB–NaCl droplets over NaCl droplets would be the photosensitizing components. Given the complexity and the lack of a method to quantify PSs in BB aerosols, using the total TOC concentration as an upper limit for estimating PS concentration is considered a compromise that allows systematic comparison. The sulfate formation reported here can be considered the lower limit of photosensitizing capacity. Our goal is to compare the photosensitizing ability in different chemical systems but not to quantify their absolute values.

State-of-the-art mass spectrometry analysis including UHPLC–Orbitrap MS and GC × GC–MS showed the existence of possible PSs such as PAHs (e.g., fluoranthene, pyrene, cyclopenta[*cd*]pyrene, 4-methylphenanthrene, benzo[*a*]pyrene, perylene; Table S2) and aromatic carbonyls (SyrAld, VL, 3,4-dimethoxybenzaldehyde, acetophenone, acetosyringone; Table S2). Photosensitizing components can directly or indirectly (by forming secondary oxidants in the presence of oxygen) oxidize S(IV) to S(VI). X. Wang et al. (2020) proposed a direct oxidation process of S(IV) to sulfate by excited triplet states of photosensitizers (^{3}PS*). To explore the contribution of the direct ^{3}PS* oxidation to sulfate formation, we performed the same sets of experiments in N_2-saturated condition, shown in Fig. S4. Under N_2-saturated conditions, secondary oxidants such as HO_2• and the OH• oxidation pathway can be ruled out due to the lack of oxygen. Chlorine radicals from droplets can also react with dissolved SO_2 to generate sulfite radicals, but O_2 is required to form sulfate. Despite initial molecular oxygen in the droplets possibly also participating in sulfate formation under N_2-saturated conditions, its contributions are likely minimal. Consequently, the sulfate formed under N_2-saturated conditions can be considered the upper limit of direct ^{3}PS* oxidation. The BB–NaCl droplets showed a direct ^{3}PS* oxidation contribution of only 3.6 % to 22.7 %, highlighting the predominant role of secondary oxidants (Tang et al., 2023). For BB_F–NaCl droplets, the contribution of direct ^{3}PS* followed the trend of WS_F–NaCl (22.7 %) > RS_F–NaCl (15.7 %) > CS_F–NaCl (7.0 %), while for BB_A–NaCl droplets, WS_A–NaCl (10.2 %) > CS_A–NaCl (6.7 %) > RS_A–NaCl (3.6 %) was observed. In summary, regardless of whether fresh or aged, the secondary oxidants triggered by indirect ^{3}PS* oxidation were the main reason for sulfate formation, highlighting the importance of O_2 in ^{3}PS*-mediated oxidation processes.

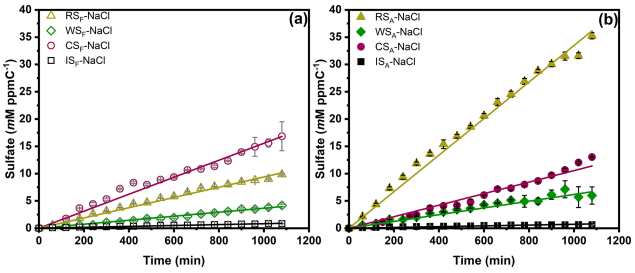

Figure 1. Sulfate production under different droplet compositions as a function of time: **(a)** fresh BB–NaCl droplets and **(b)** aged BB–NaCl droplets in air at 80 % RH. RS, WS, CS, and IS represent rice straw, wheat straw, corn straw, and incense burning, respectively. The subscripts F and A represent fresh and aged, respectively.

3.2 Aging effects on sulfate formation across various BB materials

To investigate the aging effects on sulfate formation across various BB materials, we subjected the collected BB filters to OH radical aging by irradiating them with UV lights at wavelengths of 185 and 254 nm. This combination effectively generated OH radicals (Tang et al., 2023). Figure S5 exhibits the differences in sulfate formation rates in droplets of different fresh and aged BB materials. RS and WS show sulfate formation enhancement, while CS and IS show reduction after aging. Figure 2a shows that the 18 h sulfate enhancement

Table 1. Sulfate formation rate ($k_{SO_4^{2-}}$) and the reactive (γ_{SO_2}) and normalized SO_2 uptake coefficient ($n\gamma_{SO_2}$) at various particle compositions at 80 % RH as well as sulfate formation rate ($k_{SO_4^{2-}}$) using different BB extracts and model compounds in bulk aqueous reactions. The numbers 1, 10, 100, and 200 represent the concentration of different compounds (in ppm). Additional abbreviations: Pyz, pyrazine; 4-NC, 4-nitrocatechol.

Droplet experiments			
Particle composition	$k_{SO_4^{2-}}$ ($\mu M\,min^{-1}\,(ppmC)^{-1}$)	γ_{SO_2}	$n\gamma_{SO_2}$ ($(ppmC)^{-1}$)
RS_F–NaCl	9.4 ± 0.10	$(2.2 \pm 0.023) \times 10^{-6}$	$(6.2 \pm 0.066) \times 10^{-8}$
WS_F–NaCl	3.7 ± 0.048	$(0.66 \pm 0.0086) \times 10^{-6}$	$(2.0 \pm 0.027) \times 10^{-8}$
CS_F–NaCl	15.6 ± 0.11	$(2.0 \pm 0.015) \times 10^{-6}$	$(8.8 \pm 0.065) \times 10^{-8}$
IS_F–NaCl	0.83 ± 0.011	$(1.7 \pm 0.034) \times 10^{-6}$	$(0.61 \pm 0.012) \times 10^{-8}$
RS_A–NaCl	33.5 ± 0.38	$(6.6 \pm 0.074) \times 10^{-6}$	$(21.5 \pm 0.24) \times 10^{-8}$
WS_A–NaCl	6.2 ± 0.18	$(0.92 \pm 0.027) \times 10^{-6}$	$(3.5 \pm 0.10) \times 10^{-8}$
CS_A–NaCl	10.6 ± 0.23	$(1.0 \pm 0.023) \times 10^{-6}$	$(6.2 \pm 0.13) \times 10^{-8}$
IS_A–NaCl	0.72 ± 0.026	$(1.3 \pm 0.052) \times 10^{-6}$	$(0.46 \pm 0.017) \times 10^{-8}$
Bulk aqueous experiments			
Aqueous reactions	Concentration (ppm)	$k_{SO_4^{2-}}$ ($ppm\,min^{-1}\,(ppmC)^{-1}$)	$k_{SO_4^{2-}}$ ($\mu M\,min^{-1}\,(ppmC)^{-1}$)
RS_F	1	0.31	3.2
RS_F–NaCl	1–100	0.16	1.6
RS_F–NaCl	1–200	0.085	0.9
WS_F	1	0.19	2.0
CS_F	1	0.25	2.6
IS_F	1	0.19	2.0
RS_A	1	0.33	3.4
RS_A–NaCl	1–100	0.37	3.8
RS_A–NaCl	1–200	0.63	6.4
WS_A	1	0.26	2.7
CS_A	1	0.33	3.4
IS_A	1	0.080	0.82
NaCl	100	0.051	0.52
NaCl	200	0.079	0.81
SyrAld	1	0.15	1.5
SyrAld–Pyz	1–1	0.68	7.1
SyrAld–Pyz–NaCl	1–1–10	0.67	6.9
SyrAld–Pyz–NaCl	1–1–100	0.55	5.7
SyrAld–Pyz–NaCl	1–1–200	0.50	5.2
SyrAld–4-NC	1–1	0.11	1.1
SyrAld–4-NC–NaCl	1–1–10	0.13	1.4
SyrAld–4-NC–NaCl	1–1–100	0.13	1.4
SyrAld–4-NC–NaCl	1–1–200	0.15	1.5
SyrAld–NaCl	1–10	0.11	1.1
SyrAld–NaCl	1–100	0.17	1.8
SyrAld–NaCl	1–200	0.17	1.7
VL	1	0.26	2.7
VL–Pyz	1–1	0.61	6.4
VL–Pyz–NaCl	1–1–10	0.55	5.8
VL–Pyz–NaCl	1–1–100	0.43	4.5
VL–Pyz–NaCl	1–1–200	0.42	4.3
VL–4-NC	1–1	0.17	1.7
VL–4-NC–NaCl	1–1–10	0.22	2.3
VL–4-NC–NaCl	1–1–100	0.27	2.7
VL–4-NC–NaCl	1–1–200	0.23	2.4
VL–NaCl	1–10	0.25	2.6
VL–NaCl	1–100	0.26	2.7
VL–NaCl	1–200	0.28	2.9

* The $n\gamma_{SO_2}$ was calculated by normalizing the γ_{SO_2} with the TOC concentration in the BB extracts; i.e., $n\gamma_{SO_2} = \gamma_{SO_2}/TOC$.

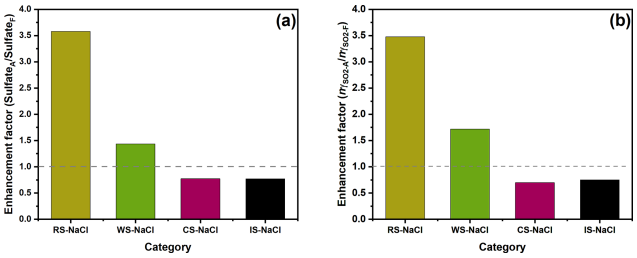

Figure 2. Enhancement factor of **(a)** sulfate and **(b)** normalized SO_2 uptake coefficient $n\gamma_{SO_2}$ between fresh and aged BB–NaCl droplets.

factor ($Sulfate_A$ / $Sulfate_F$) followed the trend of RS–NaCl (3.6) > WS–NaCl (1.4) > CS–NaCl (0.8) ≈ IS–NaCl (0.8), which is not consistent with the trends of sulfate formation for BB_F–NaCl or BB_A–NaCl, indicating the varying effects of the aging of BB materials. A similar trend was found for $n\gamma_{SO_2}$, showing the highest and lowest sulfate enhancement for RS–NaCl (3.5) and IS–NaCl (0.7), respectively.

Bulk aqueous reactions using fresh/aged BB extracts without NaCl were performed to investigate the aging effects on the sulfate formation in the cloud phase (Fig. S6). As the experiment proceeded, sulfate concentrations accumulated while bisulfite concentrations decreased. Concurrently, the pH of the aqueous solution decreased from approximately 5.0 to 3.0, reflecting enhanced acidity. Bulk reactions have lower sulfate formation rates than droplets reactions, which may be attributed to the accelerated reactions induced by PSs at the air–water interface (W. Wang et al., 2024; Martins-Costa et al., 2022), as well as the differences in concentrations of S(IV) and NaCl between bulk and droplet surfaces. However, given that interfacial reactions are closely linked to particle size (Wei et al., 2020; Chen et al., 2022b), additional research is needed to better understand their influence. Our experiments involve large droplets of the size of 60 µm. The interfacial effects of such large droplets may not be evident. Future work to examine the interfacial effects of submicron- and nanometer-sized particles is needed.

3.3 Chemical characterization of BB extracts and sulfate formation in bulk aqueous solutions

In bulk experiments, all BB extracts have higher $k_{SO_4^{2-}}$ values after aging. The increased sulfate formation of BB extracts after aging may be due to changes in their chemical compositions. Compared to RS_F (28.3 % for CHON− and 67.3 % for CHN+ in total intensity), RS_A has higher CHON− (36.1 %) and CHN+ (88.3 %) percentages (Figs. S7–S8). Zhao et al. (2022) observed a slight increase in the CHON percentage for RS from 53.4 % to 56.2 % after aging. A similar trend was observed for CS extracts, where the CHON− and CHN+ percentage increases from 26.7 % and 65.2 % to 31.5 % and 68.8 %, respectively, after aging. To semi-qualitatively distinguish BrC chromophores from the rest of dissolved organic carbon, we used the double-bond equivalent (DBE) value in the range of $0.5C \leq DBE \leq 0.9C$ as a criterion (Lin et al., 2018). For example, RS_{A-BrC} denotes the BrC chromophores in RS_A according to the above. Larger intensity fractions of CHON− species were found in RS_{A-BrC} (41.9 %) and CS_{A-BrC} (35.5 %) than RS_{F-BrC} (32.3 %) and CS_{F-BrC} (34.7 %). One of the key categories of CHON− is nitrated aromatics, which have been widely identified in lab-generated BB smoke (R.-J. Huang et al., 2022; X. Wang et al., 2017; Zhang et al., 2022; Xie et al., 2019) and field campaigns (Salvador et al., 2021; Mohr et al., 2013; Chen et al., 2022a). A series of CHON− species, e.g., $C_6H_5NO_3$, $C_6H_5NO_4$, $C_7H_7NO_3$, and $C_8H_9NO_3$, which were tentatively identified as nitrophenol, nitrocatechol, methyl-nitrophenol, and dimethyl-nitrophenol, have been detected in our BB extracts. Nitrophenol photolysis has been found to be a potential source of OH radicals (Sangwan and Zhu, 2018; Guo and Li, 2023; Cheng et al., 2009; Sangwan and Zhu, 2016), and it may partially contribute to the increase in sulfate formation by RS_A and CS_A.

Approximately 80 % of the CHN+ species identified exhibited a diatomic nitrogen composition in their molecular formula. The precise determination of the molecular structures of these compounds solely based on elemental composition is challenging due to the presence of stable isomers. However, the N bases, which contain two nitrogen atoms, can be attributed to various N-heterocyclic alkaloids (Fig. S9). For example, homologs of $C_5H_6N_2(CH_2)_n$ were likely pyrazine, pyrimidine, or aminopyridine, which are composed of six-membered heterocyclic rings with N atoms and alkyl side chains (Lin et al., 2012; Laskin et al., 2009). $C_5H_8N_2(CH_2)_n$ were likely alkyl-substituted imidazole compounds, featuring a five-membered heterocyclic ring with two nitrogen atoms as the core structure and alkyl side chains (Lin et al., 2012; Laskin et al., 2009). For $C_7H_6N_2(CH_2)_n$ homologs, the core skeleton was $C_7H_6N_2$, with an AI_{mod} of 0.8, indicating its distinctive characteristics of compounds containing fused five-membered and six-membered rings, such as benzimidazole or indazole (Y. Wang et al., 2017). Redox-inactive heterocyclic nitrogen-containing bases, e.g., pyridine, imidazole, and their derivatives, have been shown to enhance the redox activity of the humic-like substance (HULIS) fraction by hydrogen-atom transfer, with the degree of enhancement directly correlated to their concentrations (Dou et al., 2015; Kipp et al., 2004). Thus, the increased CHN+ percentage may also contribute to the enhanced sulfate formation of RS_A and CS_A by acting as an H-bond acceptor to facilitate the $^3PS^*$-mediated oxidation by generating more oxidants.

However, the CHON− and CHN+ percentages in WS_A were lower than in WS_F, indicating that the sulfate enhancement in WS_A was not due to the CHON and CHN species. Instead, CHO− accounted for a higher proportion in WS_A (68.5 %) and WS_{A-BrC} (68.9 %) than in WS_F (65.0 %) and

WS_{F-BrC} (64.8 %). This aligns with a prior aerosol mass spectrometer (AMS) study showing increased CHO proportions in aged wheat burning emissions (Fang et al., 2017). We suppose that CHO− compounds, particularly photosensitizing compounds with carbonyl groups, would explain the difference in sulfate formation in WS extracts (Gómez Alvarez et al., 2012; Go et al., 2023; Felber et al., 2020; Fu et al., 2015). Therefore, we filtered the chemical formula of CHO− species from UHPLC–Orbitrap HRMS by applying the maximum carbonyl ratio (MCR) (Y. Zhang et al., 2021; K. Wang et al., 2024; Calderon-Arrieta et al., 2024; D. Liu et al., 2023), H/C, and O/C as well as the modified aromaticity index (AI_{mod}) to focus on potential PSs (Zherebker et al., 2022; Koch and Dittmar, 2006). In short, molecular formulae were classified into six groups, namely, condensed aromatics ($AI_{mod} \geq 0.67$), polyphenolic compounds ($0.50 < AI_{mod} < 0.67$), highly unsaturated and phenolic compounds ($AI_{mod} \leq 0.5$, $H/C < 1.5$), aliphatics ($H/C \geq 1.5$, $O/C \leq 0.9$, $N = 0$), peptide-like compounds ($H/C \geq 1.5$, $O/C \leq 0.9$, $N > 0$), and sugar-like compounds ($H/C \geq 1.5$, $O/C > 0.9$); details can be found in Sect. S1. As aliphatics, peptide-like compounds, and sugar-like compounds are unlikely to be PSs, we exclude them as potential PSs. By applying further data filtration involving CHO−, condensed aromatics, polyphenolic compounds, and highly unsaturated and phenolic compounds based on the aforementioned criteria, as well as $MCR \geq 0.9$ (which includes oxidized unsaturated and highly unsaturated compounds such as PS-like imidazole-2-carboxaldehyde (2-IC) and PAHs) (Y. Zhang et al., 2021), 52.6 % and 49.7 % of the compounds (by intensity) can be considered potential PSs in WS_A and WS_F, respectively. The main compositional difference lies in polyphenolic compounds, comprising 26.3 % and 21.8 % of WS_A and WS_F, respectively. Therefore, the higher sulfate formation in WS_A may be related to the higher contributions of the polyphenolic compounds, e.g., $C_8H_8O_3$.

To summarize, we propose that in aqueous reactions, the enhanced sulfate formation in CS_A and RS_A was likely due to the increased proportions (by intensity) of CHON and CHN species, potentially nitrophenols and N-heterocyclic compounds. Conversely, the increased sulfate formation in WS_A appears to be linked to a higher percentage of CHO species. However, an association between detailed chemical characteristics and sulfate formation is not able to be discerned in this study due to the complexity of the interactions between different chemical categories and difficulties in the interpretation of the coefficients. Future studies are needed to elucidate the relationships between sulfate formation and the chemical characteristics.

3.4 Effects of chloride and nitrogen-containing species on sulfate formation

Unlike the droplet experiments where RS–NaCl has the highest sulfate enhancement factor after aging, aqueous reaction results (without NaCl) show a sulfate enhancement trend of WS > CS > RS > IS, suggesting that chloride may have an effect in the droplet experiments, especially in the RS–NaCl system. To evaluate the effects of chloride on sulfate formation, we conducted bulk reaction experiments using RS extracts as an example with 100–200 ppm NaCl additions, where the NaCl-to-TOC ratio ranged from 100 : 1 to 200 : 1 to match the range of 100 : 1 to 1000 : 1 in droplet experiments. Interestingly, incorporating NaCl yielded contrasting results for RS_F and RS_A (Fig. 3). While the addition of NaCl enhanced sulfate formation in RS_A, it showed the opposite trend in RS_F. The nature of the cations and ionic strength may affect the sulfate formation rate; however, previous studies have indicated that their effects are negligible (Zhang and Chan, 2024; Parker and Mitch, 2016). The opposite effect of the NaCl addition on RS_F and RS_A, to some extent, explains the significantly higher sulfate and SO_2 uptake coefficient enhancement factor for RS–NaCl in Fig. 2. Compared to the RS-based system, the NaCl control experiment showed minimum (but non-zero) sulfate formation (Table 1 and Fig. 3). On one hand, it supported the findings that chloride participated in the sulfate formation under light conditions but no sulfate formation under dark conditions (Cao et al., 2024; Tang et al., 2023; Zhang and Chan, 2024). On the other hand, the opposite trend of Cl^- effects on RS_F and RS_A reflects its complex interactions with BB extracts under light and air conditions. While direct reaction between S(IV) species and $^3PS^*$ may occur (X. Wang et al., 2020), other pathways, i.e., interactions among halide ions, PSs, and oxygen, should also be considered. Detailed mechanisms will be discussed later.

Statistical analysis using the Spearman correlation coefficients, as guided by the Shapiro–Wilk test (Table S4), revealed that the CHO, CHON, and CHN species exhibited significant correlations ($|R| > 0.7$) with the sulfate formation rate ($p < 0.01$, Fig. S10). While PSs can be the main CHO species contributing to sulfate formation, N-containing organic compounds (NOCs), i.e., CHN and CHON species, may affect the chloride contribution to the sulfate formation rate. Therefore, we selected SyrAld and VL as model CHO species (PSs), pyrazine (Pyz) as a model CHN, and 4-nitrocatechol (4-NC) as a model CHON to elucidate how the N-containing species can alter the effects of chloride on sulfate formation rate by studying the $CHO + Cl^-$, $CHO + CHN + Cl^-$, and $CHO + CHON + Cl^-$ systems. For SyrAld and VL, as the $[Cl^-]_0/[PS]_0$ increases, $k_{SO_4^{2-}}$ initially decreases and then increases. The initial decrease in $k_{SO_4^{2-}}$ may be attributed to the quenching of $^3PS^*$ by electron transfer from Cl^- or the loss of OH radials by forming $ClOH^{\bullet-}$ through the reaction of $OH\bullet + Cl^- \leftrightarrow ClOH^{\bullet-}$ (Anastasio and Newberg, 2007). Excessive chloride (e.g., 100 and 200 ppm) may generate Cl and OH radicals through photoexcitation in the presence of air and water and compensate for the loss of $^3PS^*$ or OH radicals. Previous studies have shown a contradictory influence of halides on the photosen-

sitized oxidation of organic compounds or bisulfite. Parker and Mitch (2016) and Zhang et al. (2023) attributed the significantly higher photodegradation of dienes, thioethers, and acetaminophen to the formation of reactive halogen species generated by the reactions of PSs and halides. Zhang and Chan (2024) reported that $[Cl^-/PS]_0$ in the range of 1 : 2 to 4 : 1 did not lead to significant differences in sulfate formation. The differences between the current results and the aforementioned study might be attributed to the higher $[Cl^-/PS]_0$ ratio used in this study (up to 200 : 1), which may have been sufficient to initiate the relevant reactions, as well as the difference in photosensitizing capacities of the PSs studied (triplet quantum yield of 0.86 ± 0.05 for 2-IC and 0.21 ± 0.01 for VL) (Felber et al., 2021, 2020). Safiarian et al. (2023) reported that increasing chloride concentrations facilitated anthracene photosensitization by producing high-level reactive oxygen species (ROS). N. Wang et al. (2023) found that the effects of chloride on sulfate formation depended on the specific PS: enhancing sulfate production for benzophenone (BP) and 3,4-dimethoxybenzaldehyde (DMB) but decreasing it for 1,4-naphthoquinone.

Incorporating CHN species yielded a 2- to 3-fold increase in $k_{SO_4^{2-}}$ due to the enhanced H transfer by CHN acting as an H-bond acceptor (Dou et al., 2015). With the addition of NaCl, the enhanced H-transfer effect by CHN was inhibited, possibly due to the consumption of ^{3}PS* by Cl^-. On the other hand, the addition of model CHON species into PSs decreased $k_{SO_4^{2-}}$ due to the consumption of ^{3}PS* by CHON species, in agreement with Y. Wang et al. (2023), who reported an increased effective quantum yield of 4-NC under co-photolysis with VL. Further addition of NaCl increased the $k_{SO_4^{2-}}$, possibly due to the consumption of 4-NC by reactive chlorine species (RCS; T. Wang et al., 2024), which, to some extent, reduced the loss of ^{3}PS*. Generally, the addition of chloride increased $k_{SO_4^{2-}}$ values of PS–CHON but decreased $k_{SO_4^{2-}}$ values of PS–CHN. However, the ambient air is characterized by the presence of tens of thousands of chemical compounds. As a result, the interplay among this diverse array of species may occur in ways that exceed current understanding, necessitating additional research to investigate the interactions between different organic compounds more thoroughly.

3.5 Proposed mechanism for sulfate formation

A conceptual diagram of PS- and chloride-mediated ROS and RCS production in the oxidation of S(IV) to S(VI) is shown in Fig. 4. Initially, the PSs (e.g., SyrAld and VL) absorb solar radiation and produce the singlet state ^{1}PS*, which then undergoes a spin conversion through intersystem crossing, leading to the formation of the triplet state ^{3}PS*. The ^{3}PS* can react with molecular oxygen through energy transfer and generate singlet state $^1O_2$*, while the ^{3}PS* returns to ground state. The $^1O_2$* can then transform to $O_2^{\bullet-}$ via electron transfer. The ^{3}PS* can also react with an H donor (RH, e.g., organic acids, syringol, guaiacol; Table S3), leading to the formation of the alkyl or phenoxy radical (R•) and the ketyl radical (PSH•). R• can react with O_2 and form RO_2 radicals, while PSH• can transfer an H atom to O_2 and form $HO_2^{\bullet}$, returning to its ground state PS. Additionally, ^{3}PS* can react with an electron donor, e.g., Cl^-, and form chlorine radicals and $PS^{\bullet-}$. The $PS^{\bullet-}$ formed then reacts with O_2 and forms $O_2^{\bullet-}$, which undergoes a series of reactions and forms $HO_2\bullet$, H_2O_2, and OH•. $RO_2\bullet$ can further react with $RO_2\bullet$ or $HO_2\bullet$ and form organic peroxides (ROOR/ROOH). The abovementioned reactions are the main processes in the ROS pathway. Recently, Zhang and Chan (2024) proposed that the reactive chlorine species (RCS) would contribute to sulfate formation. Cao et al. (2024) proposed a mechanism of OH and Cl radicals formation by $[Cl^-–H_3O^+–O_2]$ under light irradiation through an electron transfer process. Our results also demonstrate that the addition of Cl^- will affect the oxidation process of S(VI) (Figs. 3, S11–S13). Combining the above, the RCS pathway is shown in orange arrows in Fig. 4. The Cl• can be formed in two pathways, photoexcitation of the $[Cl^-–H_3O^+–O_2]$ complex that generates Cl radicals in deliquescent BB–NaCl droplets or aqueous BB–NaCl solution (Cao et al., 2024) and ^{3}PS*-mediated Cl• formation via electron transfer by Cl^- (Corral Arroyo et al., 2019). The Cl• radicals formed can then react with each other through radical–radical reactions and produce molecular Cl_2. The $Cl^{\bullet-}$ can also react with Cl^- or $Cl_2^{\bullet-}$, forming $Cl_2^{\bullet-}$ or Cl_2. Cl• and $Cl_2^{\bullet-}$ can also react with OH and form HOCl. The ^{3}PS* itself can also oxidize the S(IV) (e.g., dissolved SO_2 or

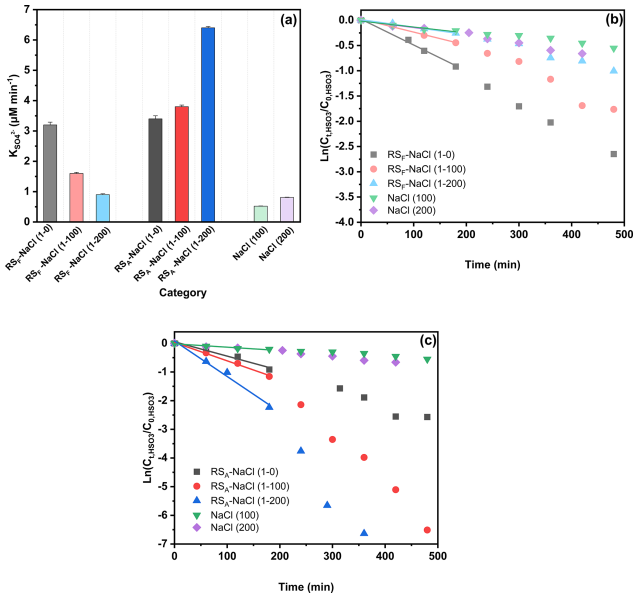

Figure 3. **(a)** The sulfate formation rate and **(b, c)** bisulfite decay in RS–NaCl aqueous reactions. The terms "1-0", "1-100", and "1-200" refer to the concentration ratios of TOC_{RS} and NaCl, in which 1, 100, and 200 represent 1, 100, and 200 ppm, respectively.

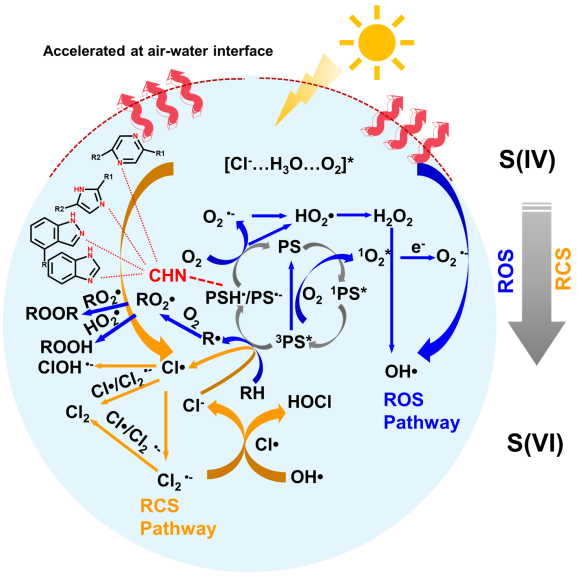

Figure 4. Conceptual diagram of PS- and chloride-mediated ROS and RCS production in the oxidation processes from S(IV) to S(VI).

bisulfite) to S(VI). However, significantly lower sulfate formation was found in the presence of N_2 than air (Fig. S4), highlighting the importance of secondary oxidants compared to direct ^{3}PS* oxidation. As a consequence, these reactive species, e.g., $OH^\bullet$ / $HO_2^\bullet$ / $RO_2^\bullet$ / $O_2^{\bullet-}$ / ROOH / ROOR and $Cl^\bullet$ / $Cl_2^{\bullet-}$, may all participate in the oxidation of S(IV) to S(VI). In addition, nitrogen-containing heterocyclic compounds such as pyrazine can act as H-bond acceptors and facilitate the H transfer, which then generates more ROS (Dou et al., 2015). Note that although ROS and RCS pathways both contribute to the oxidation from S(IV) to S(VI), they may act in competitive relationships due to the co-consumption of ^{3}PS*. Therefore, different Cl effects may occur regarding various combinations of reactants (Fig. 3, promoting effect on RS_A and inhibiting effects on RS_F).

4 Atmospheric implications

This study provided laboratory evidence that the PSs in biomass burning extracts can enhance the sulfate formation in NaCl particles, primarily by triggering the formation of secondary oxidants under light and air conditions, with a lower contribution of direct photosensitization via triplets (evidenced by N_2 atmosphere, Fig. S4). The sulfate formation rates of BB_F–NaCl particles were ~10-fold higher than those of IS_F–NaCl, following the trend of CS_F–NaCl > RS_F–NaCl > WS_F–NaCl > IS_F–NaCl. Upon UV exposure, the sulfate formation trend shifted to RS_A–NaCl > CS_A–NaCl > WS_A–NaCl > IS_A–NaCl, which might be explained by the effects of chloride (evidenced by aqueous reactions, Fig. 3 and Table 1). Interestingly, the incorporation of Cl^- into bulk solutions increased the sulfate formation rate in RS_A, while it decreased it in RS_F. This seems to be different from our group's previous work, where no significant sulfate formation rate was found with the addition of Cl^- (Zhang and Chan, 2024). The difference can be explained by the following.

1. *Differences in PS/Cl^-*. The prior study might have used an insufficient PS/Cl^- ratio (2 : 1–1 : 4), while the current one significantly expanded it to 1 : 200.

2. *Differences in photosensitizing capacity.* The former study used a strong PS, while the current study focused on the real BB (using TOC as a metric, with only a small portion of TOC considered PSs).

3. *The complexity of the reaction system.* The former study focused on mixing two individual species, while in real BB extracts, more complicated reactions may occur.

Furthermore, our results using model PSs show that although additional model CHN species would increase the sulfate formation by expedited H transfer via acting as H-bond acceptors, the addition of chloride could inhibit the sulfate formation rate, suggesting that the RCS pathway was less efficient in sulfate formation compared to the ROS pathway in the PS–CHN bulk system (Figs. S11 and S12).

While our prior study has examined the potential interplay between chloride and PSs at limited mixing ratios (up to 4 : 1 in bulk solution) (Zhang and Chan, 2024), this work expanded the Cl^-/PS ratio to a broader range (200 : 1) and systematically identified the interactions among different organics, including PSs, NOCs, and chloride, using sulfate formation as a compass. This highlights the importance of studying secondary aerosol formation in mixed experimental systems under an air pollution complex. Our work suggests that in coastal regions heavily influenced by anthropogenic emissions like biomass burning, especially those near rice-growing regions or affected by transported wildfire smoke, such as Guangdong, Fujian, and Taiwan, the transported BB plumes together with the high RH (Cheung et al., 2015) and abundant reactive gases could play an important role in sulfate and potentially secondary organic aerosol formation.

Data availability. Datasets are available upon request to the corresponding author, Chak K. Chan (chak.chan@kaust.edu.sa).

Supplement. The supplement related to this article is available online at: https://doi.org/10.5194/acp-25-425-2025-supplement.

Author contributions. RT and CKC conceptualized and designed the study. YQ and YC collected the samples. RT performed the experiments and data analysis and wrote the draft. JM provided assistance in data processing. All the authors reviewed and edited the paper and contributed to scientific discussions.

Competing interests. The contact author has declared that none of the authors has any competing interests.

Acknowledgements. The authors thank the University Research Facility in Chemical and Environmental Analysis (UCEA) at The Hong Kong Polytechnic University for the use of its UHPLC–Orbitrap mass spectrometer and Sirius Tse and Chi Hang Chow for assistance with sample analyses.

Financial support. This research has been supported by the Hong Kong Research Grants Council (grant no. 11314222); National Natural Science Foundation of China (grant no. 42107115); and Natural Science Foundation of Shandong Province, China (grant no. ZR2021QD111). Chak K. Chan was also supported by the KAUST baseline research fund (grant no. BAS/1/1432-01-01) and KAUST Center of Excellence for Smart Health (KCSH) fund (grant no. 5932).

Review statement. This paper was edited by Sergey A. Nizkorodov and reviewed by Xinke Wang and two anonymous referees.

References

Alexander, B., Allman, D. J., Amos, H. M., Fairlie, T. D., Dachs, J., Hegg, D. A., and Sletten, R. S.: Isotopic constraints on the formation pathways of sulfate aerosol in the marine boundary layer of the subtropical northeast Atlantic Ocean, J. Geophys. Res.-Atmos., 117, D06304, https://doi.org/10.1029/2011JD016773, 2012.

Anastasio, C. and Newberg, J. T.: Sources and sinks of hydroxyl radical in sea-salt particles, J. Geophys. Res.-Atmos., 112, D10306, https://doi.org/10.1029/2006JD008061, 2007.

Andreae, M. O.: Emission of trace gases and aerosols from biomass burning – an updated assessment, Atmos. Chem. Phys., 19, 8523–8546, https://doi.org/10.5194/acp-19-8523-2019, 2019.

Bond, T. C., Doherty, S. J., Fahey, D. W., Forster, P. M., Berntsen, T., DeAngelo, B. J., Flanner, M. G., Ghan, S., Kärcher, B., Koch, D., Kinne, S., Kondo, Y., Quinn, P. K., Sarofim, M. C., Schultz, M. G., Schulz, M., Venkataraman, C., Zhang, H., Zhang, S., Bellouin, N., Guttikunda, S. K., Hopke, P. K., Jacobson, M. Z., Kaiser, J. W., Klimont, Z., Lohmann, U., Schwarz, J. P., Shindell, D., Storelvmo, T., Warren, S. G., and Zender, C. S.: Bounding the role of black carbon in the climate system: A scientific assessment, J. Geophys. Res.-Atmos., 118, 5380–5552, https://doi.org/10.1002/jgrd.50171, 2013.

Cai, J., Zeng, X., Zhi, G., Gligorovski, S., Sheng, G., Yu, Z., Wang, X., and Peng, P.: Molecular composition and photochemical evolution of water-soluble organic carbon (WSOC) extracted from field biomass burning aerosols using high-resolution mass spectrometry, Atmos. Chem. Phys., 20, 6115–6128, https://doi.org/10.5194/acp-20-6115-2020, 2020.

Calderon-Arrieta, D., Morales, A. C., Hettiyadura, A. P. S., Estock, T. M., Li, C., Rudich, Y., and Laskin, A.: Enhanced Light Absorption and Elevated Viscosity of Atmospheric Brown Carbon through Evaporation of Volatile Components, Environ. Sci. Technol., 58, 7493–7504, https://doi.org/10.1021/acs.est.3c10184, 2024.

Cao, Y., Liu, J., Ma, Q., Zhang, C., Zhang, P., Chen, T., Wang, Y., Chu, B., Zhang, X., Francisco, J. S., and He, H.: Photoactivation of Chlorine and Its Catalytic Role in the Formation of Sulfate Aerosols, J. Am. Chem. Soc., 146, 1467–1475, https://doi.org/10.1021/jacs.3c10840, 2024.

Chen, J., Li, C., Ristovski, Z., Milic, A., Gu, Y., Islam, M. S., Wang, S., Hao, J., Zhang, H., He, C., Guo, H., Fu, H., Miljevic, B., Morawska, L., Thai, P., Lam, Y. F., Pereira, G., Ding, A., Huang, X., and Dumka, U. C.: A review of biomass burning: Emissions and impacts on air quality, health and climate in China, Sci. Total Environ., 579, 1000–1034, https://doi.org/10.1016/j.scitotenv.2016.11.025, 2017.

Chen, Y., Zheng, P., Wang, Z., Pu, W., Tan, Y., Yu, C., Xia, M., Wang, W., Guo, J., Huang, D., Yan, C., Nie, W., Ling, Z., Chen, Q., Lee, S., and Wang, T.: Secondary Formation and Impacts of Gaseous Nitro-Phenolic Compounds in the Continental Outflow Observed at a Background Site in South China, Environ. Sci. Technol., 56, 6933–6943, https://doi.org/10.1021/acs.est.1c04596, 2022a.

Chen, Z., Liu, P., Wang, W., Cao, X., Liu, Y.-X., Zhang, Y.-H., and Ge, M.: Rapid Sulfate Formation via Uncatalyzed Autoxidation of Sulfur Dioxide in Aerosol Microdroplets, Environ. Sci. Technol., 56, 7637–7646, https://doi.org/10.1021/acs.est.2c00112, 2022b.

Cheng, S.-B., Zhou, C.-H., Yin, H.-M., Sun, J.-L., and Han, K.-L.: OH produced from o-nitrophenol photolysis: A combined experimental and theoretical investigation, The J. Chem. Phys., 130, 234311, https://doi.org/10.1063/1.3152635, 2009.

Cheung, H. H., Yeung, M. C., Li, Y. J., Lee, B. P., and Chan, C. K.: Relative humidity-dependent HTDMA measurements of ambient aerosols at the HKUST supersite in Hong Kong, China, Aerosol Sci. Technol., 49, 643–654, 2015.

Chi, J. W., Li, W. J., Zhang, D. Z., Zhang, J. C., Lin, Y. T., Shen, X. J., Sun, J. Y., Chen, J. M., Zhang, X. Y., Zhang, Y. M., and Wang, W. X.: Sea salt aerosols as a reactive surface for inorganic and organic acidic gases in the Arctic troposphere, Atmos. Chem. Phys., 15, 11341–11353, https://doi.org/10.5194/acp-15-11341-2015, 2015.

Corral Arroyo, P., Aellig, R., Alpert, P. A., Volkamer, R., and Ammann, M.: Halogen activation and radical cycling initiated by imidazole-2-carboxaldehyde photochemistry, Atmos. Chem. Phys., 19, 10817–10828, https://doi.org/10.5194/acp-19-10817-2019, 2019.

Dang, C., Segal-Rozenhaimer, M., Che, H., Zhang, L., Formenti, P., Taylor, J., Dobracki, A., Purdue, S., Wong, P.-S., Nenes, A., Sedlacek III, A., Coe, H., Redemann, J., Zuidema, P., Howell, S., and Haywood, J.: Biomass burning and marine aerosol processing over the southeast Atlantic Ocean: a TEM

single-particle analysis, Atmos. Chem. Phys., 22, 9389–9412, https://doi.org/10.5194/acp-22-9389-2022, 2022.

Dou, J., Lin, P., Kuang, B.-Y., and Yu, J. Z.: Reactive Oxygen Species Production Mediated by Humic-like Substances in Atmospheric Aerosols: Enhancement Effects by Pyridine, Imidazole, and Their Derivatives, Environ. Sci. Technol., 49, 6457–6465, https://doi.org/10.1021/es5059378, 2015.

Fang, Z., Deng, W., Zhang, Y., Ding, X., Tang, M., Liu, T., Hu, Q., Zhu, M., Wang, Z., Yang, W., Huang, Z., Song, W., Bi, X., Chen, J., Sun, Y., George, C., and Wang, X.: Open burning of rice, corn and wheat straws: primary emissions, photochemical aging, and secondary organic aerosol formation, Atmos. Chem. Phys., 17, 14821–14839, https://doi.org/10.5194/acp-17-14821-2017, 2017.

Felber, T., Schaefer, T., and Herrmann, H.: Five-Membered Heterocycles as Potential Photosensitizers in the Tropospheric Aqueous Phase: Photophysical Properties of Imidazole-2-carboxaldehyde, 2-Furaldehyde, and 2-Acetylfuran, The J. Phys. Chem. A, 124, 10029–10039, https://doi.org/10.1021/acs.jpca.0c07028, 2020.

Felber, T., Schaefer, T., He, L., and Herrmann, H.: Aromatic Carbonyl and Nitro Compounds as Photosensitizers and Their Photophysical Properties in the Tropospheric Aqueous Phase, The J. Phys. Chem. A, 125, 5078–5095, https://doi.org/10.1021/acs.jpca.1c03503, 2021.

Fu, H., Ciuraru, R., Dupart, Y., Passananti, M., Tinel, L., Rossignol, S., Perrier, S., Donaldson, D. J., Chen, J., and George, C.: Photosensitized Production of Atmospherically Reactive Organic Compounds at the Air/Aqueous Interface, J. Am. Chem. Soc., 137, 8348–8351, https://doi.org/10.1021/jacs.5b04051, 2015.

Fushimi, A., Saitoh, K., Hayashi, K., Ono, K., Fujitani, Y., Villalobos, A. M., Shelton, B. R., Takami, A., Tanabe, K., and Schauer, J. J.: Chemical characterization and oxidative potential of particles emitted from open burning of cereal straws and rice husk under flaming and smoldering conditions, Atmos. Environ., 163, 118–127, https://doi.org/10.1016/j.atmosenv.2017.05.037, 2017.

Gantt, B. and Meskhidze, N.: The physical and chemical characteristics of marine primary organic aerosol: a review, Atmos. Chem. Phys., 13, 3979–3996, https://doi.org/10.5194/acp-13-3979-2013, 2013.

Gen, M., Zhang, R., Huang, D. D., Li, Y., and Chan, C. K.: Heterogeneous Oxidation of SO_2 in Sulfate Production during Nitrate Photolysis at 300 nm: Effect of pH, Relative Humidity, Irradiation Intensity, and the Presence of Organic Compounds, Environ. Sci. Technol., 53, 8757–8766, https://doi.org/10.1021/acs.est.9b01623, 2019a.

Gen, M., Zhang, R., Huang, D. D., Li, Y., and Chan, C. K.: Heterogeneous SO_2 Oxidation in Sulfate Formation by Photolysis of Particulate Nitrate, Environ. Sci. Technol. Lett., 6, 86–91, https://doi.org/10.1021/acs.estlett.8b00681, 2019b.

Go, B. R., Lyu, Y., Ji, Y., Li, Y. J., Huang, D. D., Li, X., Nah, T., Lam, C. H., and Chan, C. K.: Aqueous secondary organic aerosol formation from the direct photosensitized oxidation of vanillin in the absence and presence of ammonium nitrate, Atmos. Chem. Phys., 22, 273–293, https://doi.org/10.5194/acp-22-273-2022, 2022.

Go, B. R., Li, Y. J., Huang, D. D., Wang, Y., and Chan, C. K.: Comparison of aqueous secondary organic aerosol (aqSOA) product distributions from guaiacol oxidation by non-phenolic and phenolic methoxybenzaldehydes as photosensitizers in the absence and presence of ammonium nitrate, Atmos. Chem. Phys., 23, 2859–2875, https://doi.org/10.5194/acp-23-2859-2023, 2023.

Gómez Alvarez, E., Wortham, H., Strekowski, R., Zetzsch, C., and Gligorovski, S.: Atmospheric Photosensitized Heterogeneous and Multiphase Reactions: From Outdoors to Indoors, Environ. Sci. Technol., 46, 1955–1963, https://doi.org/10.1021/es2019675, 2012.

Guo, S. and Li, H.: Photolysis of nitrophenols in gas phase and aqueous environment: a potential daytime source for atmospheric nitrous acid (HONO), Environ. Sci. Atmos., 3, 143–155, 2023.

Hu, W., Zhou, H., Chen, W., Ye, Y., Pan, T., Wang, Y., Song, W., Zhang, H., Deng, W., Zhu, M., Wang, C., Wu, C., Ye, C., Wang, Z., Yuan, B., Huang, S., Shao, M., Peng, Z., Day, D. A., Campuzano-Jost, P., Lambe, A. T., Worsnop, D. R., Jimenez, J. L., and Wang, X.: Oxidation Flow Reactor Results in a Chinese Megacity Emphasize the Important Contribution of S/IVOCs to Ambient SOA Formation, Environ. Sci. Technol., 56, 6880–6893, https://doi.org/10.1021/acs.est.1c03155, 2022.

Huang, G., Wang, S., Chang, X., Cai, S., Zhu, L., Li, Q., and Jiang, J.: Emission factors and chemical profile of I/SVOCs emitted from household biomass stove in China, Sci. Total Environ., 842, 156940, https://doi.org/10.1016/j.scitotenv.2022.156940, 2022.

Huang, R.-J., Yang, L., Shen, J., Yuan, W., Gong, Y., Ni, H., Duan, J., Yan, J., Huang, H., You, Q., and Li, Y. J.: Chromophoric Fingerprinting of Brown Carbon from Residential Biomass Burning, Environ. Sci. Technol. Lett., 9, 102–111, https://doi.org/10.1021/acs.estlett.1c00837, 2022.

Huang, S., Wu, Z., Poulain, L., van Pinxteren, M., Merkel, M., Assmann, D., Herrmann, H., and Wiedensohler, A.: Source apportionment of the organic aerosol over the Atlantic Ocean from 53° N to 53° S: significant contributions from marine emissions and long-range transport, Atmos. Chem. Phys., 18, 18043–18062, https://doi.org/10.5194/acp-18-18043-2018, 2018.

Jiang, H., Carena, L., He, Y., Wang, Y., Zhou, W., Yang, L., Luan, T., Li, X., Brigante, M., Vione, D., and Gligorovski, S.: Photosensitized Degradation of DMSO Initiated by PAHs at the Air-Water Interface, as an Alternative Source of Organic Sulfur Compounds to the Atmosphere, J. Geophys. Res.-Atmos., 126, e2021JD035346, https://doi.org/10.1029/2021JD035346, 2021.

Jones, M. W., Abatzoglou, J. T., Veraverbeke, S., Andela, N., Lasslop, G., Forkel, M., Smith, A. J. P., Burton, C., Betts, R. A., van der Werf, G. R., Sitch, S., Canadell, J. G., Santín, C., Kolden, C., Doerr, S. H., and Le Quéré, C.: Global and Regional Trends and Drivers of Fire Under Climate Change, Rev. Geophys., 60, e2020RG000726, https://doi.org/10.1029/2020RG000726, 2022.

Kalogridis, A. C., Popovicheva, O. B., Engling, G., Diapouli, E., Kawamura, K., Tachibana, E., Ono, K., Kozlov, V. S., and Eleftheriadis, K.: Smoke aerosol chemistry and aging of Siberian biomass burning emissions in a large aerosol chamber, Atmos/ Environ/, 185, 15–28, https://doi.org/10.1016/j.atmosenv.2018.04.033, 2018.

Kim, Y. H., Warren, S. H., Krantz, Q. T., King, C., Jaskot, R., Preston, W. T., George, B. J., Hays, M. D., Landis, M. S., and Higuchi, M.: Mutagenicity and lung toxicity of smoldering vs. flaming emissions from various biomass fuels: implications for health effects from wildland fires, Environ. Health Perspect., 126, 017011, https://doi.org/10.1289/EHP2200, 2018.

Kim, Y. H., Warren, S. H., Kooter, I., Williams, W. C., George, I. J., Vance, S. A., Hays, M. D., Higuchi, M. A., Gavett, S. H., DeMarini, D. M., Jaspers, I., and Gilmour, M. I.: Chemistry, lung toxicity and mutagenicity of burn pit smoke-related particulate matter, Part. Fibre Toxicol., 18, 45, https://doi.org/10.1186/s12989-021-00435-w, 2021.

Kipp, B. H., Faraj, C., Li, G., and Njus, D.: Imidazole facilitates electron transfer from organic reductants, Bioelectrochemistry, 64, 7–13, https://doi.org/10.1016/j.bioelechem.2003.12.010, 2004.

Koch, B. P. and Dittmar, T.: From mass to structure: An aromaticity index for high© – resolution mass data of natural organic matter, Rapid Commun. Mass Sp., 20, 926–932, 2006.

Laskin, A., Smith, J. S., and Laskin, J.: Molecular Characterization of Nitrogen-Containing Organic Compounds in Biomass Burning Aerosols Using High-Resolution Mass Spectrometry, Environ. Sci. Technol., 43, 3764–3771, https://doi.org/10.1021/es803456n, 2009.

Li, F., Zhou, S., Zhao, J., Hang, J., Lu, H., Li, X., Gao, M., Li, Y., and Wang, X.: Aqueous Photosensitization of Syringaldehyde: Reactivity, Effects of Environmental Factors, and Formation of Brown Carbon Products, ACS Earth and Space Chemistry, 8, 1193–1203, https://doi.org/10.1021/acsearthspacechem.4c00004, 2024.

Li, S., Jiang, X., Roveretto, M., George, C., Liu, L., Jiang, W., Zhang, Q., Wang, W., Ge, M., and Du, L.: Photochemical aging of atmospherically reactive organic compounds involving brown carbon at the air–aqueous interface, Atmos. Chem. Phys., 19, 9887–9902, https://doi.org/10.5194/acp-19-9887-2019, 2019.

Liang, Z., Li, Y., Go, B. R., and Chan, C. K.: Complexities of Photosensitization in Atmospheric Particles, ACS ES&T Air, 1, 1333–1351, https://doi.org/10.1021/acsestair.4c00112, 2024.

Lin, P., Rincon, A. G., Kalberer, M., and Yu, J. Z.: Elemental Composition of HULIS in the Pearl River Delta Region, China: Results Inferred from Positive and Negative Electrospray High Resolution Mass Spectrometric Data, Environ. Sci. Technol., 46, 7454–7462, https://doi.org/10.1021/es300285d, 2012.

Lin, P., Fleming, L. T., Nizkorodov, S. A., Laskin, J., and Laskin, A.: Comprehensive Molecular Characterization of Atmospheric Brown Carbon by High Resolution Mass Spectrometry with Electrospray and Atmospheric Pressure Photoionization, Anal. Chem., 90, 12493–12502, https://doi.org/10.1021/acs.analchem.8b02177, 2018.

Liu, D., Zhang, Y., Zhong, S., Chen, S., Xie, Q., Zhang, D., Zhang, Q., Hu, W., Deng, J., Wu, L., Ma, C., Tong, H., and Fu, P.: Large differences of highly oxygenated organic molecules (HOMs) and low-volatile species in secondary organic aerosols (SOAs) formed from ozonolysis of β-pinene and limonene, Atmos. Chem. Phys., 23, 8383–8402, https://doi.org/10.5194/acp-23-8383-2023, 2023.

Liu, H., Pei, X., Zhang, F., Song, Y., Kuang, B., Xu, Z., and Wang, Z.: Relative Humidity Dependence of Growth Factor and Real Refractive Index for Sea Salt/Malonic Acid Internally Mixed Aerosols, J. Geophys. Res.-Atmos., 128, e2022JD037579, https://doi.org/10.1029/2022JD037579, 2023.

Liu, Y., Wang, T., Fang, X., Deng, Y., Cheng, H., Nabi, I., and Zhang, L.: Brown carbon: An underlying driving force for rapid atmospheric sulfate formation and haze event, Sci. Total Environ., 734, 139415, https://doi.org/10.1016/j.scitotenv.2020.139415, 2020.

Mao, J., Ren, X., Brune, W. H., Olson, J. R., Crawford, J. H., Fried, A., Huey, L. G., Cohen, R. C., Heikes, B., Singh, H. B., Blake, D. R., Sachse, G. W., Diskin, G. S., Hall, S. R., and Shetter, R. E.: Airborne measurement of OH reactivity during INTEX-B, Atmos. Chem. Phys., 9, 163–173, https://doi.org/10.5194/acp-9-163-2009, 2009.

Martins-Costa, M. T., Anglada, J. M., Francisco, J. S., and Ruiz-López, M. F.: Photosensitization mechanisms at the air–water interface of aqueous aerosols, Chem. Sci., 13, 2624–2631, 2022.

Mohr, C., Lopez-Hilfiker, F. D., Zotter, P., Prévôt, A. S. H., Xu, L., Ng, N. L., Herndon, S. C., Williams, L. R., Franklin, J. P., Zahniser, M. S., Worsnop, D. R., Knighton, W. B., Aiken, A. C., Gorkowski, K. J., Dubey, M. K., Allan, J. D., and Thornton, J. A.: Contribution of Nitrated Phenols to Wood Burning Brown Carbon Light Absorption in Detling, United Kingdom during Winter Time, Environ. Sci. Technol., 47, 6316–6324, https://doi.org/10.1021/es400683v, 2013.

Parker, K. M. and Mitch, W. A.: Halogen radicals contribute to photooxidation in coastal and estuarine waters, P. Natl. Acad. Sci. USA, 113, 5868–5873, 2016.

Peng, Z. and Jimenez, J. L.: Radical chemistry in oxidation flow reactors for atmospheric chemistry research, Chem. Soc. Rev., 49, 2570–2616, 2020.

Pozzoli, L., Gilardoni, S., Perrone, M. G., de Gennaro, G., de Rienzo, M., and Vione, D.: POLYCYCLIC AROMATIC HYDROCARBONS IN THE ATMOSPHERE: MONITORING, SOURCES, SINKS AND FATE. I: MONITORING AND SOURCES, Ann. Chim., 94, 17–33, https://doi.org/10.1002/adic.200490002, 2004.

Qin, Y., Wang, H., Wang, Y., Lu, X., Tang, H., Zhang, J., Li, L., and Fan, S.: Wildfires in Southeast Asia pollute the atmosphere in the northern South China Sea, Sci. Bull., 69, 1011–1015, https://doi.org/10.1016/j.scib.2024.02.026, 2024.

Qiu, Y., Wu, X., Zhang, Y., Xu, L., Hong, Y., Chen, J., Chen, X., and Deng, J.: Aerosol light absorption in a coastal city in Southeast China: Temporal variations and implications for brown carbon, J. Environ. Sci., 80, 257–266, https://doi.org/10.1016/j.jes.2019.01.002, 2019.

Rao, X. and Collett, J. L. J. : Behavior of S (IV) and formaldehyde in a chemically heterogeneous cloud, Environ. Sci. Technol., 29, 1023–1031, 1995.

Rowe, J. P., Lambe, A. T., and Brune, W. H.: Technical Note: Effect of varying the $\lambda = 185$ and 254 nm photon flux ratio on radical generation in oxidation flow reactors, Atmos. Chem. Phys., 20, 13417–13424, https://doi.org/10.5194/acp-20-13417-2020, 2020.

Ruiz-Lopez, M. F., Francisco, J. S., Martins-Costa, M. T. C., and Anglada, J. M.: Molecular reactions at aqueous interfaces, Nat. Rev. Chem., 4, 459–475, https://doi.org/10.1038/s41570-020-0203-2, 2020.

Safiarian, M. S., Ugboya, A., Khan, I., Marichev, K. O., and Grant, K. B.: New Insights into the Phototoxicity of Anthracene-Based Chromophores: The Chloride Salt Effect, Chem. Res. Toxicol., 36, 1002–1020, https://doi.org/10.1021/acs.chemrestox.2c00235, 2023.

Salvador, C. M. G., Tang, R., Priestley, M., Li, L., Tsiligiannis, E., Le Breton, M., Zhu, W., Zeng, L., Wang, H., Yu, Y., Hu, M.,

Guo, S., and Hallquist, M.: Ambient nitro-aromatic compounds – biomass burning versus secondary formation in rural China, Atmos. Chem. Phys., 21, 1389–1406, https://doi.org/10.5194/acp-21-1389-2021, 2021.

Sangwan, M. and Zhu, L.: Absorption cross sections of 2-nitrophenol in the 295–400 nm region and photolysis of 2-nitrophenol at 308 and 351 nm, The J. Phys. Chem. A, 120, 9958–9967, 2016.

Sangwan, M. and Zhu, L.: Role of Methyl-2-nitrophenol Photolysis as a Potential Source of OH Radicals in the Polluted Atmosphere: Implications from Laboratory Investigation, The J. Phys. Chem. A, 122, 1861–1872, https://doi.org/10.1021/acs.jpca.7b11235, 2018.

Song, J., Li, M., Zou, C., Cao, T., Fan, X., Jiang, B., Yu, Z., Jia, W., and Peng, P. a.: Molecular Characterization of Nitrogen-Containing Compounds in Humic-like Substances Emitted from Biomass Burning and Coal Combustion, Environ. Sci. Technol., 56, 119–130, https://doi.org/10.1021/acs.est.1c04451, 2022.

Song, K., Tang, R., Li, A., Wan, Z., Zhang, Y., Gong, Y., Lv, D., Lu, S., Tan, Y., Yan, S., Yan, S., Zhang, J., Fan, B., Chan, C. K., and Guo, S.: Particulate organic emissions from incense-burning smoke: Chemical compositions and emission characteristics, Sci. Total Environ., 897, 165319, https://doi.org/10.1016/j.scitotenv.2023.165319, 2023.

Tang, R., Zhang, R., Ma, J., Song, K., Mabato, B. R. G., Cuevas, R. A. I., Zhou, L., Liang, Z., Vogel, A. L., Guo, S., and Chan, C. K.: Sulfate Formation by Photosensitization in Mixed Incense Burning–Sodium Chloride Particles: Effects of RH, Light Intensity, and Aerosol Aging, Environ/ Sci/ Technol/, 57, 10295–10307, https://doi.org/10.1021/acs.est.3c02225, 2023.

Teich, M., van Pinxteren, D., Kecorius, S., Wang, Z., and Herrmann, H.: First quantification of imidazoles in ambient aerosol particles: potential photosensitizers, brown carbon constituents, and hazardous components, Environ. Sci. Technol., 50, 1166-1173, 2016.

Ting, Y., Mitchell, E. J. S., Allan, J. D., Liu, D., Spracklen, D. V., Williams, A., Jones, J. M., Lea-Langton, A. R., McFiggans, G., and Coe, H.: Mixing State of Carbonaceous Aerosols of Primary Emissions from "Improved" African Cookstoves, Environ. Sci. Technol., 52, 10134–10143, https://doi.org/10.1021/acs.est.8b00456, 2018.

Tkacik, D. S., Lambe, A. T., Jathar, S., Li, X., Presto, A. A., Zhao, Y., Blake, D., Meinardi, S., Jayne, J. T., Croteau, P. L., and Robinson, A. L.: Secondary Organic Aerosol Formation from in-Use Motor Vehicle Emissions Using a Potential Aerosol Mass Reactor, Environ. Sci. Technol., 48, 11235–11242, https://doi.org/10.1021/es502239v, 2014.

van Pinxteren, M., Fiedler, B., van Pinxteren, D., Iinuma, Y., Körtzinger, A., and Herrmann, H.: Chemical characterization of sub-micrometer aerosol particles in the tropical Atlantic Ocean: marine and biomass burning influences, J. Atmos. Chem., 72, 105–125, https://doi.org/10.1007/s10874-015-9307-3, 2015.

Wang, K., Zhang, Y., Tong, H., Han, J., Fu, P., Huang, R.-J., Zhang, H., and Hoffmann, T.: Molecular-Level Insights into the Relationship between Volatility of Organic Aerosol Constituents and $PM_{2.5}$ Air Pollution Levels: A Study with Ultrahigh-Resolution Mass Spectrometry, Environ. Sci. Technol., 58, 7947–7957, https://doi.org/10.1021/acs.est.3c10662, 2024.

Wang, N., Zhou, D., Liu, H., Tu, Y., Ma, Y., and Li, Y.: Triplet-Excited Dissolved Organic Matter Efficiently Promoted Atmospheric Sulfate Production: Kinetics and Mechanisms, Separations, 10, 335, https://doi.org/10.3390/separations10060335, 2023.

Wang, S., Liu, T., Jang, J., Abbatt, J. P. D., and Chan, A. W. H.: Heterogeneous interactions between SO_2 and organic peroxides in submicron aerosol, Atmos. Chem. Phys., 21, 6647–6661, https://doi.org/10.5194/acp-21-6647-2021, 2021.

Wang, T., Deng, L., Tan, C., Hu, J., and Singh, R. P.: Comparative analysis of chlorinated disinfection byproducts formation from 4-nitrophenol and 2-amino-4-nitrophenol during UV/post-chlorination, Sci. Total Environ., 927, 172200, https://doi.org/10.1016/j.scitotenv.2024.172200, 2024.

Wang, W., Liu, Y., Wang, T., Ge, Q., Li, K., Liu, J., You, W., Wang, L., Xie, L., Fu, H., Chen, J., and Zhang, L.: Significantly Accelerated Photosensitized Formation of Atmospheric Sulfate at the Air–Water Interface of Microdroplets, J. Am. Chem. Soc., 146, 6580–6590, https://doi.org/10.1021/jacs.3c11892, 2024.

Wang, X., Gemayel, R., Baboomian, V. J., Li, K., Boreave, A., Dubois, C., Tomaz, S., Perrier, S., Nizkorodov, S. A., and George, C.: Naphthalene-derived secondary organic aerosols interfacial photosensitizing properties, Geophys. Res. Lett., 48, e2021GL093465, https://doi.org/10.1029/2021GL093465, 2021.

Wang, X., Gu, R., Wang, L., Xu, W., Zhang, Y., Chen, B., Li, W., Xue, L., Chen, J., and Wang, W.: Emissions of fine particulate nitrated phenols from the burning of five common types of biomass, Environ. Pollut., 230, 405–412, https://doi.org/10.1016/j.envpol.2017.06.072, 2017.

Wang, X., Gemayel, R., Hayeck, N., Perrier, S., Charbonnel, N., Xu, C., Chen, H., Zhu, C., Zhang, L., Wang, L., Nizkorodov, S. A., Wang, X., Wang, Z., Wang, T., Mellouki, A., Riva, M., Chen, J., and George, C.: Atmospheric Photosensitization: A New Pathway for Sulfate Formation, Environ. Sci. Technol., 54, 3114–3120, https://doi.org/10.1021/acs.est.9b06347, 2020.

Wang, Y., Hu, M., Xu, N., Qin, Y., Wu, Z., Zeng, L., Huang, X., and He, L.: Chemical composition and light absorption of carbonaceous aerosols emitted from crop residue burning: influence of combustion efficiency, Atmos. Chem. Phys., 20, 13721–13734, https://doi.org/10.5194/acp-20-13721-2020, 2020.

Wang, Y., Qiu, T., Zhang, C., Hao, T., Mabato, B. R. G., Zhang, R., Gen, M., Chan, M. N., Huang, D. D., and Ge, X.: Co-photolysis of mixed chromophores affects atmospheric lifetimes of brown carbon, Environ. Sci.-Atmos., 3, 1145–1158, 2023.

Wang, Y., Hu, M., Lin, P., Guo, Q., Wu, Z., Li, M., Zeng, L., Song, Y., Zeng, L., Wu, Y., Guo, S., Huang, X., and He, L.: Molecular Characterization of Nitrogen-Containing Organic Compounds in Humic-like Substances Emitted from Straw Residue Burning, Environ. Sci. Technol., 51, 5951–5961, https://doi.org/10.1021/acs.est.7b00248, 2017.

Wei, Z., Li, Y., Cooks, R. G., and Yan, X.: Accelerated reaction kinetics in microdroplets: Overview and recent developments, Ann. Rev. Phys. Chem., 71, 31–51, 2020.

Wu, C.-H., Yuan, C.-S., Yen, P.-H., Yeh, M.-J., and Soong, K.-Y.: Diurnal and seasonal variation, chemical characteristics, and source identification of marine fine particles at two remote islands in South China Sea: A superimposition effect of local emissions and long-range transport, Atmos. Environ., 270, 118889, https://doi.org/10.1016/j.atmosenv.2021.118889, 2022.

Xie, M., Chen, X., Hays, M. D., and Holder, A. L.: Composition and light absorption of N-containing aromatic compounds in organic aerosols from laboratory biomass burning, Atmos. Chem. Phys., 19, 2899–2915, https://doi.org/10.5194/acp-19-2899-2019, 2019.

Yang, M., Zhang, H., Chang, F., and Hu, X.: Self-sensitized photochlorination of benzo[a]pyrene in saline water under simulated solar light irradiation, J. Hazard. Mater., 408, 124445, https://doi.org/10.1016/j.jhazmat.2020.124445, 2021.

Yao, M., Zhao, Y., Hu, M., Huang, D., Wang, Y., Yu, J. Z., and Yan, N.: Multiphase reactions between secondary organic aerosol and sulfur dioxide: kinetics and contributions to sulfate formation and aerosol aging, Environ. Sci. Technol. Lett., 6, 768–774, 2019.

Ye, C., Lu, K., Song, H., Mu, Y., Chen, J., and Zhang, Y.: A critical review of sulfate aerosol formation mechanisms during winter polluted periods, J. Environ. Sci., 123, 387–399, https://doi.org/10.1016/j.jes.2022.07.011, 2023.

Ye, J., Abbatt, J. P. D., and Chan, A. W. H.: Novel pathway of SO_2 oxidation in the atmosphere: reactions with monoterpene ozonolysis intermediates and secondary organic aerosol, Atmos. Chem. Phys., 18, 5549–5565, https://doi.org/10.5194/acp-18-5549-2018, 2018.

You, B., Li, S., Tsona, N. T., Li, J., Xu, L., Yang, Z., Cheng, S., Chen, Q., George, C., Ge, M., and Du, L.: Environmental Processing of Short-Chain Fatty Alcohols Induced by Photosensitized Chemistry of Brown Carbons, ACS Earth Space Chem., 4, 631–640, https://doi.org/10.1021/acsearthspacechem.0c00023, 2020.

Zhang, L., Hu, B., Liu, X., Luo, Z., Xing, R., Li, Y., Xiong, R., Li, G., Cheng, H., Lu, Q., Shen, G., and Tao, S.: Variabilities in Primary N-Containing Aromatic Compound Emissions from Residential Solid Fuel Combustion and Implications for Source Tracers, Environ. Sci. Technol., 56, 13622–13633, https://doi.org/10.1021/acs.est.2c03000, 2022.

Zhang, R. and Chan, C. K.: Simultaneous formation of sulfate and nitrate via co-uptake of SO_2 and NO_2 by aqueous NaCl droplets: combined effect of nitrate photolysis and chlorine chemistry, Atmos. Chem. Phys., 23, 6113–6126, https://doi.org/10.5194/acp-23-6113-2023, 2023.

Zhang, R. and Chan, C. K.: Enhanced Sulfate Formation through Synergistic Effects of Chlorine Chemistry and Photosensitization in Atmospheric Particles, ACS ES&T Air, 1, 92–102, https://doi.org/10.1021/acsestair.3c00030, 2024.

Zhang, R., Gen, M., Huang, D., Li, Y., and Chan, C. K.: Enhanced Sulfate Production by Nitrate Photolysis in the Presence of Halide Ions in Atmospheric Particles, Environ. Sci. Technol., 54, 3831–3839, https://doi.org/10.1021/acs.est.9b06445, 2020.

Zhang, S., Li, D., Ge, S., Wu, C., Xu, X., Liu, X., Li, R., Zhang, F., and Wang, G.: Elucidating the Mechanism on the Transition-Metal Ion-Synergetic-Catalyzed Oxidation of SO_2 with Implications for Sulfate Formation in Beijing Haze, Environ. Sci. Technol., 58, 2912–2921, https://doi.org/10.1021/acs.est.3c08411, 2024.

Zhang, S., Li, D., Ge, S., Liu, S., Wu, C., Wang, Y., Chen, Y., Lv, S., Wang, F., Meng, J., and Wang, G.: Rapid sulfate formation from synergetic oxidation of SO_2 by O_3 and NO_2 under ammonia-rich conditions: Implications for the explosive growth of atmospheric $PM_{2.5}$ during haze events in China, Sci. Total Environ., 772, 144897, https://doi.org/10.1016/j.scitotenv.2020.144897, 2021.

Zhang, T., Dong, J., Zhang, C., Kong, D., Ji, Y., Zhou, Q., and Lu, J.: Photo-transformation of acetaminophen sensitized by fluoroquinolones in the presence of bromide, Chemosphere, 327, 138525, https://doi.org/10.1016/j.chemosphere.2023.138525, 2023.

Zhang, Y., Wang, K., Tong, H., Huang, R.-J., and Hoffmann, T.: The maximum carbonyl ratio (MCR) as a new index for the structural classification of secondary organic aerosol components, Rapid Commun. Mass Spectro., 35, e9113, https://doi.org/10.1002/rcm.9113, 2021.

Zhang, Y., Bao, F., Li, M., Xia, H., Huang, D., Chen, C., and Zhao, J.: Photoinduced Uptake and Oxidation of SO_2 on Beijing Urban $PM_{2.5}$, Environ. Sci. Technol., 54, 14868–14876, https://doi.org/10.1021/acs.est.0c01532, 2020.

Zhao, R., Zhang, Q., Xu, X., Wang, W., Zhao, W., Zhang, W., and Zhang, Y.: Effect of photooxidation on size distribution, light absorption, and molecular compositions of smoke particles from rice straw combustion, Environ. Pollut., 311, 119950, https://doi.org/10.1016/j.envpol.2022.119950, 2022.

Zherebker, A., Rukhovich, G. D., Sarycheva, A., Lechtenfeld, O. J., and Nikolaev, E. N.: Aromaticity Index with Improved Estimation of Carboxyl Group Contribution for Biogeochemical Studies, Environ. Sci. Technol., 56, 2729–2737, https://doi.org/10.1021/acs.est.1c04575, 2022.

Zhong, S., Liu, R., Yue, S., Wang, P., Zhang, Q., Ma, C., Deng, J., Qi, Y., Zhu, J., and Liu, C.-Q.: Peatland Wildfires Enhance Nitrogen-Containing Organic Compounds in Marine Aerosols over the Western Pacific, Environm. Sci. Technol., 58, 10991–11002, https://doi.org/10.1021/acs.est.3c10125, 2024.

Zhou, L., Liang, Z., Go, B. R., Cuevas, R. A. I., Tang, R., Li, M., Cheng, C., and Chan, C. K.: Sulfate formation via aerosol-phase SO_2 oxidation by model biomass burning photosensitizers: 3,4-dimethoxybenzaldehyde, vanillin and syringaldehyde using single-particle mixing-state analysis, Atmos. Chem. Phys., 23, 5251–5261, https://doi.org/10.5194/acp-23-5251-2023, 2023.